# Synergistic Effects of Functionalized WS$_2$ and SiO$_2$ Nanoparticles and a Phosphonium Ionic Liquid as Hybrid Additives of Low-Viscosity Lubricants

José M. Liñeira del Río [1,2,*], Carlos M. C. G. Fernandes [2,3], David E. P. Gonçalves [2] and Jorge H. O. Seabra [3]

1 Laboratory of Thermophysical and Tribological Properties, Nafomat Group, Department of Applied Physics, Faculty of Physics, and Institute of Materials (iMATUS), Universidade de Santiago de Compostela, 15782 Santiago de Compostela, Spain

2 Unidade de Tribologia, Vibraçoes e Manutençao Industrial, INEGI, Universidade do Porto, 4200-465 Porto, Portugal; cfernandes@fe.up.pt (C.M.C.G.F.); degoncalves@inegi.up.pt (D.E.P.G.)

3 Faculdade de Engenharia, Universidade do Porto, Rua Dr. Roberto Frias s/n, 4200-465 Porto, Portugal; jseabra@inegi.up.pt

\* Correspondence: josemanuel.lineira@usc.es

**Abstract:** This research shows the antifriction and antiwear synergies between a phosphonium ionic liquid (IL) and f-WS$_2$ and f-SiO$_2$ nanoparticles (NPs) as additives of a base oil with low viscosity (PAO6). Mass concentrations of 0.1 wt% nanoadditives and 1% IL were selected to formulate the nanolubricants. Pure sliding and rolling–sliding friction tests were performed at 120 °C, finding great friction reductions in comparison with the PAO6 base oil, specifically for the double hybrid nanolubricant (PAO6 + 1 wt% IL + 0.1 wt% f-WS$_2$ + 0.1 wt% f-SiO$_2$). Regarding the wear produced, the greatest antiwear behavior was also achieved for the double hybrid nanolubricant (width reduction of 48% and worn area decrease of 84%). Furthermore, by means of Raman microscopy and roughness examination of the worn surfaces, it can be proposed that the lubrication mechanism of doubled hybrid nanolubricants could be supported by the adsorbed tribofilm (IL and f-WS$_2$) as well as the mending effects (f-WS$_2$ and f-SiO$_2$).

**Keywords:** ionic liquids; nanoparticles; friction; wear

## 1. Introduction

The worldwide emergence of electric vehicles (EV) in society has caused the need to develop technology with the aim of obtaining good performance from their systems and mechanical elements. Electric vehicle manufacturers demand new and improved lubricants that have specific properties to obtain ideal operation in severe conditions. Among the requirements demanded in comparison with conventional lubricants, we can highlight high thermal conductivity, adequate electrical conductivity to isolate and avoid destructive arcs and optimal lubricant viscosity (low viscosity), since low-viscosity lubricants produce significant savings of energy by reducing losses due to viscous shear and pumping [1]. For instance, Gupta [2] estimated the efficiency differences of a Toyota Prius adapted to work as an EV by using transmission lubricants with different viscosities, seeing that an optimal vehicle efficiency enhancement of around 17% can be reached by using the lowest-viscosity transmission oil (Lubrizol ATF, 45 cSt@40 °C and 9 cSt@100 °C, from Lubrizol, Wickliffe, Ohio, USA).

Today, lubricants that have good properties are made up of synthetic base oils since they have low viscosities, good thermal stability and good lubricity. Taking these facts into account, it can be said that this type of oil can be considered one of the best alternatives for the formulation and development of lubricants for electric vehicles. In particular, polyalphaolefin (PAO)-type base oils are the most used since they have good tribological performance at high temperatures [3]. Nevertheless, these base oils need additives to

further increase and optimize their properties as lubricants. Thus, an interesting solution is to use nanoparticles (NPs) as base oil additives, since they have shown good performance as antifriction and antiwear additives in different investigations [4–8]. There are numerous reasons to use NPs as lubricating oil additives, the most notable being their small size, which permits these particles to enter the contact area and thus cause a positive lubrication impact. Additionally, good tribological performance has been found for ionic liquids (ILs) as lubricants [9,10]. Likewise, the addition of NPs as additives to ionic liquid lubricants can increase their tribological performance [11,12]. Nonetheless, ILs are expensive, and the recent target is to use ILs as additives [13]. In this regard, ILs with phosphonium cations have demonstrated excellent performance as additives of different oils for steel/steel contacts [14,15].

One of the biggest challenges in the formulation of nanolubricants is attaining good nanolubricant temporal stability, since the NPs tend to sediment in the base oil, especially when the viscosity of the base oil is low. It is well known that ILs can also act as dispersants, improving the temporal stability of the nanolubricants [16]. By combining the required properties of ILs and NPs, improved stability and better efficiency can be reached [17–20]. These hybrid formulations of NPs and ILs as lubricant additives can exhibit interesting positive antifriction and antiwear synergies [21–25]. For instance, Upendra et al. [24] studied the tribological characteristics of a phosphonium IL with $Al_2O_3$, CuO and $SiO_2$ NPs as additives of a mineral base oil. They found interesting tribological synergies between the IL and NPs. Furthermore, Kumar and Garg [26] found interesting synergies between three different ILs and $TiO_2$ NPs as hybrid additives of rice bran oil.

Research on the combined impacts of ILs and NPs as oil additives is still insufficient, especially in the case of low-viscosity lubricants. In this study, to increase information on the collective effects of ILs and NPs as lubricant additives, the authors studied the synergies of trihexyltetradecylphosphonium bis(2-ethylhexyl)phosphate [$P_{6,6,6,14}$][DEHP], with two different functionalized NPs: tungsten disulfide, f-$WS_2$, and silicon dioxide, f-$SiO_2$, as additives of a base oil with low viscosity (PAO6). The tribological synergies between the IL and each NP (hybrid nanolubricant) were analyzed, as were the synergies between the IL and both NPs in the same lubricant formulation (double hybrid nanolubricants).

In this research, PAO6 was chosen as the base oil given its low viscosity and also its good lubricant properties. Regarding the nanoadditives, both f-$WS_2$ and f-$SiO_2$ NPs are widely used as lubricant additives in traditional base oils (not low viscosity), showing very good tribological results, both in friction and wear [27–30].

Thus, from an engineering point of view, this research could contribute to the development of low-viscosity lubricants optimized to use as transmission fluids, since commercial automatic transmission lubricants are currently still being used in this type of vehicle; therefore, the authors consider that this research is important for developing potential lubricants.

## 2. Materials and Methods

Figure 1 displays a diagram with the experimental methodology carried out in this research.
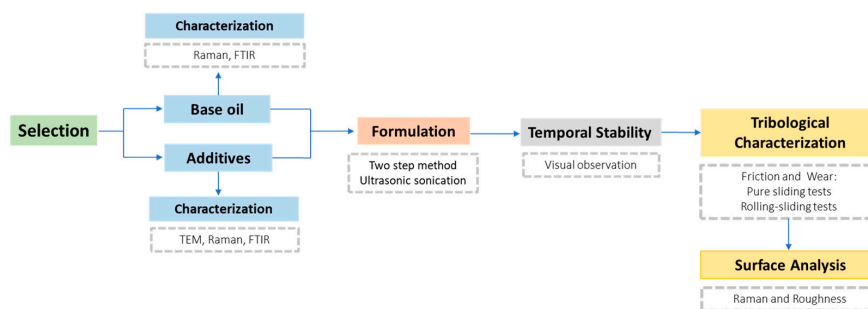


**Figure 1.** Schematic diagram with the experimental procedure of this research.

### 2.1. Base Oil and Additives

The base oil used in this research, polyalphaolefin 6 (PAO6), was provided by Repsol (Madrid, Spain). A sample of this base oil has a dynamic viscosity and density at 313.15 K of 14.25 mPa.s and 0.8033 g·cm$^{-3}$, respectively. PAO6 was earlier characterized by some techniques like infrared spectroscopy (FTIR) and Raman spectroscopy, where the typical peaks of alkyl C-C chains, as well as the bending and stretching of C-H, were observed [31].

The ionic liquid trihexyltetradecylphosphonium bis(2-ethylhexyl)phosphate [$P_{6,6,6,14}$][DEHP] (CAS-1092655-30-5), was used as a PAO6 base oil additive. This IL was provided by Iolitec (GmbH, Heilbronn, Germany) and has a purity >0.98. This IL was earlier characterized by means of FTIR and Raman spectroscopy [22]. Concerning the nanoadditives used in this research to formulate the PAO6 nanolubricants, two functionalized nanoparticles (from US Research Nanomaterials) were used: tungsten disulfide NPs coated with mineral oil (f-WS$_2$) with a 99.9% purity and a density of 7.5 g/cm$^3$ and silicon oxide NPs (f-SiO$_2$, surface coated with 3–4 wt% KH550) with a purity of 96% and a density of 2.4 g/cm$^3$. Furthermore, both NPs were characterized via many techniques. Thus, transmission electron microscopy (TEM) was utilized to study the shape and size of both NPs. Figure 2 exhibits the TEM images of the NPs used as additives and the NP size distribution for each nanoadditive. It can be observed that f-WS$_2$ NPs have a spherical shape and an average size of around 10 nm. As for f-SiO$_2$ NPs, a spherical flaky shape can be observed, and the obtained average particle size is around 15 nm.
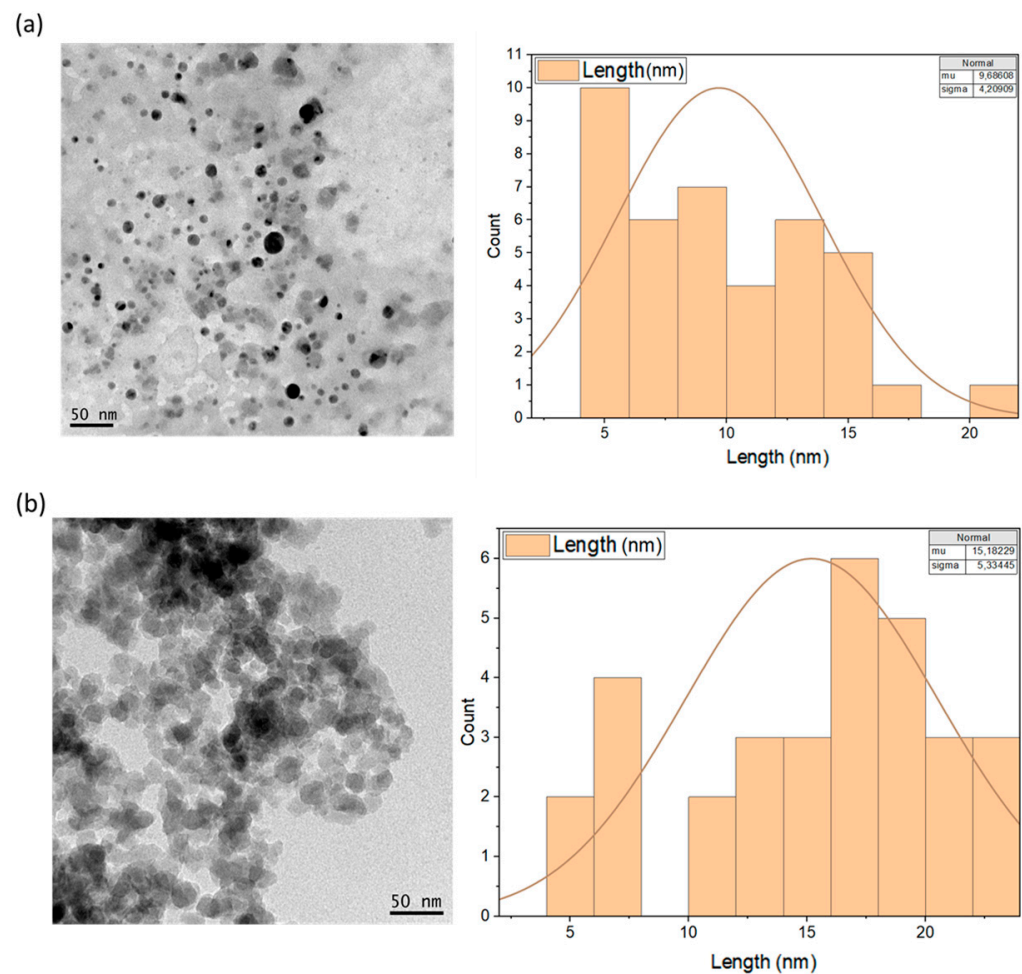


**Figure 2.** TEM characterization of (**a**) f-SiO$_2$ and (**b**) f-WS$_2$ nanopowders.

Furthermore, FTIR was employed to identify the typical bonds in f-WS$_2$ and f-SiO$_2$ NPs. Figure 3 displays the FTIR spectra of f-WS$_2$ and f-SiO$_2$ NPs. Displaying the spectrum of f-WS$_2$, Figure 3a reveals a vibrational band around 3400 cm$^{-1}$, which could be linked to atmospheric –OH. Another band around 2905 cm$^{-1}$ could be ascribed to the typical bending vibration of W-S [32]. Likewise, the band that figures at 1630 cm$^{-1}$ could be linked to the stretching vibration of O-H groups [33]. Additionally, the band placed at 1050 cm$^{-1}$ occurs owing to the S-S bond [33]. Concerning the spectrum of f-SiO$_2$ NPs, Figure 3b shows the characteristic bands of SiO$_2$ [34]. An intense band around 1100 cm$^{-1}$ is related to the stretching vibration of Si-O, and two other bands around 450 cm$^{-1}$ and 810 cm$^{-1}$ are associated with the bending vibration of Si-O. The small bands around 1700 cm$^{-1}$ are characteristic for carbonyl groups C=O. This band implies the existence of a silane coupling agent on the SiO$_2$ NP surface [35].
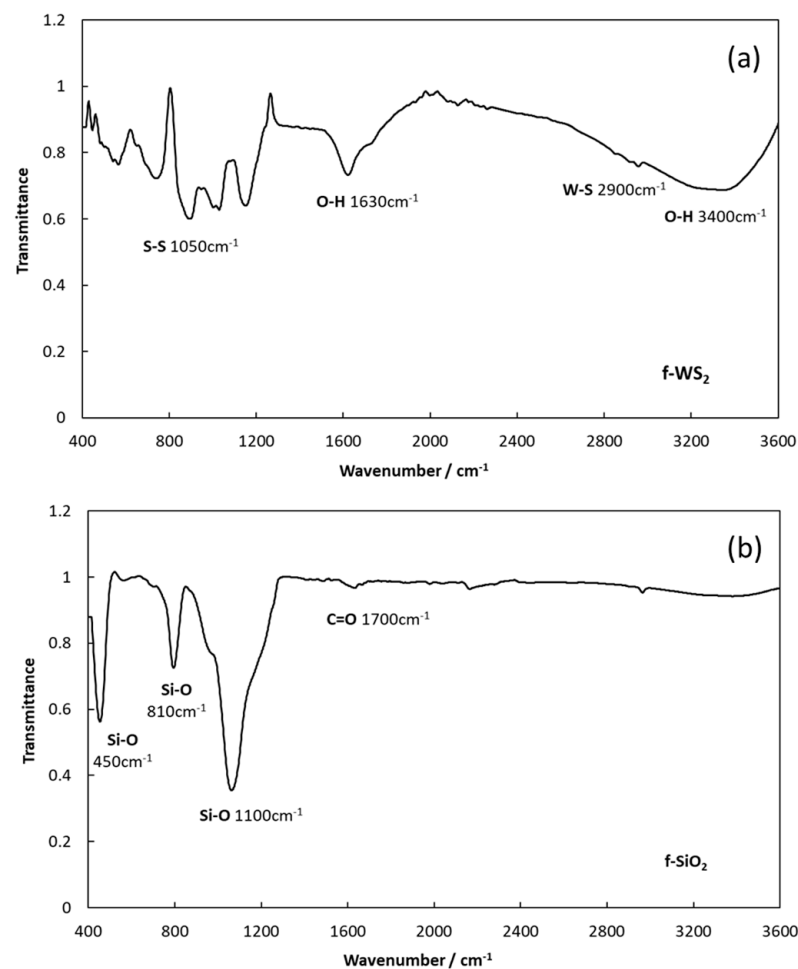


**Figure 3.** FTIR spectra of (**a**) f-WS$_2$ and (**b**) f-SiO$_2$ NPs.

Raman spectroscopy was also used to characterize the different functional groups of both NPs. Hence, the Raman spectrum of f-WS$_2$ NPs, in Figure 4a, displays the two typical peaks of E2g and A1g, located between 350 cm$^{-1}$ and 400 cm$^{-1}$, which are correlated to the in-plane vibrational mode of the S and W atoms and out-of-plane S atoms, respectively [36]. Concerning the f-SiO$_2$ NPs, the Raman spectrum, shown in Figure 4b, displays bands at 970 and 605 cm$^{-1}$, which are ascribed to the stretching mode of surface Si-OH and the D2 defect mode [37].

**Figure 4.** Raman spectra of (**a**) f-WS$_2$ and (**b**) f-SiO$_2$ NPs.

*2.2. Preparation and Stability of Nanolubricants*

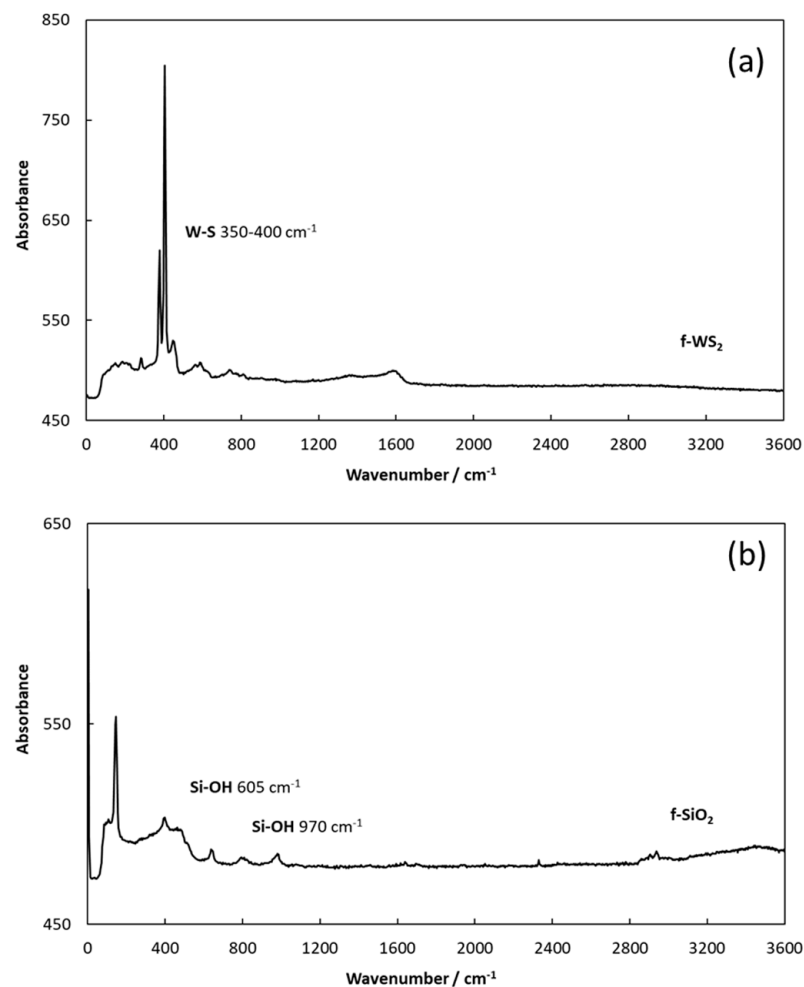Five nanodispersions were prepared apart from a mixture of PAO6 base oil and trihexyltetradecylphosphonium bis(2-ethylhexyl) phosphate (IL) with a mass concentration of 1 wt% IL. The conventional two-step procedure was utilized to formulate non-hybrid potential nanolubricants:

1.    PAO6 + 0.1 wt% f-WS$_2$.
2.    PAO6 + 0.1 wt% f-SiO$_2$.

Furthermore, to formulate the hybrid and double hybrid potential nanolubricants, the NPs were added to the IL, and then this mixture was mechanically mixed by means of an agate mortar for 10 min and then blended with the PAO6 base oil:

3.    PAO6 + 1 wt% IL + 0.1 wt% f-WS$_2$.
4.    PAO6 + 1 wt% IL + 0.1 wt% f-SiO$_2$.
5.    PAO6 + 1 wt% IL + 0.1 wt% f-WS$_2$ + 0.1 wt% f-SiO$_2$.

All nanodispersions (non-hybrid, hybrid and double hybrid) were homogenized for 4 h with an ultrasound bath, operating in the continuous mode (180 W and 37 kHz). Additionally, the mass of the NPs was measured in a Sartorius balance (model MC 210P and readability of 0.01 mg). The weight concentrations of NPs and ILs was selected according to the improved tribological performances reached in our prior articles [19,23,25]. Moreover, the stability of the above formulated potential nanolubricants was studied by means of sediment photograph capturing. Thus, Figure 5 shows the temporal stability of the above mentioned nanolubricants. It can be clearly seen that, for non-hybrid nanolubricants, the NPs tend to sediment after two weeks of nanolubricant formulation, whereas in the case of

hybrid and double hybrid nanolubricants (containing IL), the precipitation does not occur. This fact may be due to the presence of the IL, which could act as a dispersant.
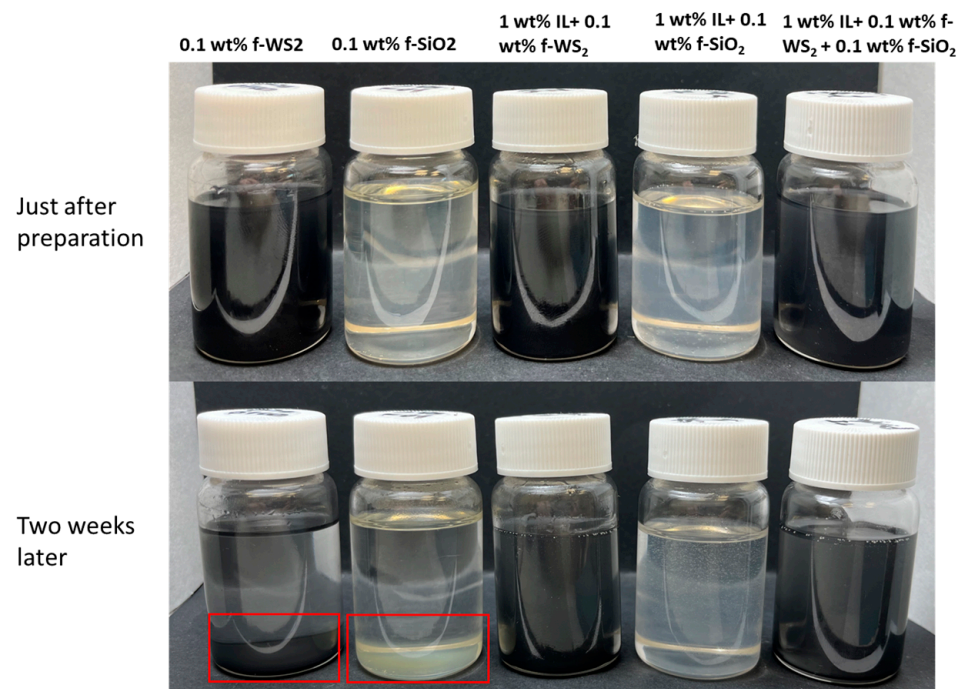


**Figure 5.** Temporal stability of PAO6-based nanolubricants (in the red square the sedimentation of the NPs).

*2.3. Tribological Tests: Pure Sliding*

Tribological friction tests with PAO6 base oil and all the dispersions mentioned above were performed with the Anton Paar MCR 302 rheometer coupled with a T-PTD200 tribology cell (Graz, Austria). This tribological device has a Peltier hood H-PTD 200 used to control the temperature. Regarding the test setup, a ball-on-three-pins configuration was chosen. More information regarding the disposition can be found in previous work [38]. The upper specimen, the ball, has a 12.7 mm diameter and a roughness of 0.04 μm (Ra), but the pins exhibit sizes of 6 mm in both diameter and height and a roughness of 0.08 μm (Ra). Pins and balls are of hardened 100Cr6 steel with a hardness of 62–66 Rockwell C. The test conditions corresponded to a boundary lubrication regime according to the lambda ratio calculated with the Hamrock and Downson formula [39] (λ value of 0.06). It should be considered that around 1.3 mL of each sample lubricant is needed to fully flood the pins. Three different replicates were performed for each sample lubricant to attain good repeatability. Regarding the test conditions, they were carried out with a sliding speed of 0.10 m/s, tribological force of 9.43 N in each pin and a testing temperature of 393.15 K. The generated wear in the pure sliding friction tests was quantified through an exhaustive 3D optical profilometer Sensofar S-Neox in different ways: wear scar diameter (WSD), wear track depth (WTD) or worn area, achieving a suitable comparison of the wear formed by the PAO6 base oil and by the non-hybrid, hybrid and double-hybrid nanodispersions. Furthermore, this profilometer was also employed to determine the worn surface roughness (Ra and Rq, through ISO4287 standard) of pins, and therefore, it helped with understanding the antiwear competence of each lubricant. Finally, the Raman WITec alpha300R+ microscope was also used in order to identify the wear mechanisms that can occur with nanolubricants and, in this way, to know how both NPs and the IL can help reduce wear and/or friction.

*2.4. Rolling–Sliding Friction Tests*

To study the antifriction behavior in different lubrication regimes with the PAO6 base oil and the above mentioned nanodispersions, a ball-on-disc EHD2 device from PCS Instruments (London, UK) was utilized. For these studies, the metal contact pair is formed by a carbon chrome steel ball (19.05 mm diameter) and a disc of carbon chrome steel. Both specimens are driven with two different electric motors to complete the tests under rolling–sliding. More details concerning this tribological apparatus can be seen in prior articles [38]. The tribological tests were carried out under completely flooded lubrication (about 150 mL of lubricant sample) at a 393.15 K operating temperature, a 50 N load (maximum Hertz pressure of 0.7 GPa) and a 5% slide/roll ratio (*SRR*):

$$SRR(\%) = 2 \times \frac{(U_{disc} - U_{ball})}{(U_{disc} + U_{ball})} \times 100 \tag{1}$$

$U_{disc}$ and $U_{ball}$ are the disc and ball speeds at the tribological contact point, respectively, whereas the entrainment speed ($U_s$) is

$$U_S = \frac{(U_{disc} + U_{ball})}{2} \tag{2}$$

To evaluate the friction behavior in different lubrication regimes, three different discs were employed (two rough and one smooth). The same speed conditions (0.05 to 2 m/s ramp) were used for each tribological friction analysis. The friction coefficient was estimated as the mean of those determined from two tribological analyses: the first with an increasing ramping speed and the second one with a decreasing speed. The properties of tribological specimens (Table 1) were supplied by the provider.

**Table 1.** Principal physical properties of discs and ball utilized in tribological tests.

| Parameters | Steel Ball | Steel Discs | | |
| --- | --- | --- | --- | --- |
| | | Smooth | Rough 1 | Rough 2 |
| Elastic modulus/GPa | 210 | 210 | 210 | 210 |
| Poisson coefficient/GPa | 0.29 | 0.29 | 0.29 | 0.29 |
| Diameter/mm | 19.05 | 100 | 100 | 100 |
| Surface roughness, Rq/nm | 20 | 20 | 100 | 300 |

## 3. Results

*3.1. Friction and Wear Findings under Pure Sliding Tests*

The mean friction coefficients observed for the base oil and the different dispersions studied under pure sliding are shown in Figure 6 and Table 2. As can be seen, for all the formulated lubricants, friction was considerably reduced compared to the PAO6 base oil, highlighting the great reductions produced for the hybrid- and double-hybrid-type nanolubricants. In particular, the best antifriction performance was observed for the double hybrid nanolubricant (PAO6 + 1 wt% IL + 0.1 wt% f-WS$_2$ + 0.1 wt% f-SiO$_2$) with a mean friction coefficient of 0.1154, whereas the one achieved for the PAO6 base oil was 0.1542, which implies a greatest friction decrease of 25%. Therefore, it can be suggested that the combination of the different lubricant additives (double hybrid), both NPs (f-WS$_2$ and f-SiO$_2$) and the IL, generated an antifriction synergy between them, which implies a good tribological performance in comparison with the non-hybrid and hybrid lubricants. Contact aging is an important phenomenon in tribology, with impacts ranging from the nanoscale to the macroscale [40,41]. Thus, when contact is kept stationary for some time, the force required to initiate sliding is usually bigger than the sliding friction, as contact aging is the transition from sliding to static friction. In this case, due to the presence of NPs and ILs, contact aging could be modified, implying a friction reduction.
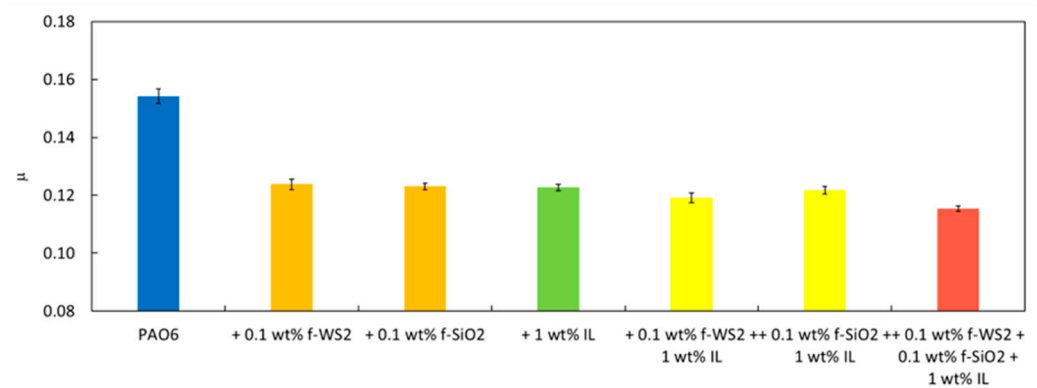
**Figure 6.** Mean friction coefficients ($\mu$) attained with PAO6 and formulated lubricants.

**Table 2.** Mean coefficients of friction, $\mu$, and mean parameters of wear: width (WSD), depth (WTD) and area with their standard deviations for the studied lubricants based on PAO6.

| Lubricant | $\mu$ | $\sigma$ | WSD/mm | $\sigma$/mm | WTD/mm | $\sigma$/mm | Area/mm$^2$ | $\sigma$/mm$^2$ |
|---|---|---|---|---|---|---|---|---|
| PAO6 | 0.1542 | 0.0026 | 435 | 10 | 2.60 | 0.19 | 806 | 65 |
| +0.1 wt% f-WS$_2$ | 0.1238 | 0.0018 | 413 | 12 | 1.74 | 0.32 | 515 | 49 |
| +0.1 wt% f-SiO$_2$ | 0.1231 | 0.0011 | 345 | 11 | 1.77 | 0.24 | 389 | 44 |
| +1 wt% IL | 0.1227 | 0.0012 | 367 | 17 | 1.94 | 0.43 | 485 | 53 |
| +0.1 wt% f-WS$_2$ + 1 wt% IL | 0.1191 | 0.0017 | 238 | 14 | 0.727 | 0.11 | 139 | 26 |
| +0.1 wt% f-SiO$_2$ + 1 wt% IL | 0.1218 | 0.0013 | 251 | 13 | 0.667 | 0.15 | 129 | 18 |
| +0.1 wt% f-WS$_2$ + 0.1 wt% f-SiO$_2$ + 1 wt% IL | 0.1154 | 0.0010 | 225 | 12 | 0.668 | 0.10 | 126 | 12 |

Regarding the wear created in the pins after the pure sliding tests, it can be seen in Figure 7 and Table 2 that all formulated sample lubricants presented a better anti-wear performance compared to unadditivated PAO6 for all the wear parameters. It is particularly extraordinary that the double hybrid nanolubricants (PAO6 + 1 wt% IL + 0.1 wt% f-WS$_2$ + 0.1 wt% f-SiO$_2$) reached the best antiwear behavior (Figures 7 and 8), with reductions of 48%, 74% and 84% for width, depth and area, respectively, compared with the PAO6 base oil. This fact indicates that, for the friction performance, the combination of the different lubricant additives (double hybrid) led to an important tribological synergy that suggests a good tribological performance compared to the base oil and the other lubricants. It should be noted that, for all the nanolubricants, an important wear reduction was also achieved in comparison to the base oil, especially for the hybrid nanolubricants (PAO6 + 1 wt% IL + 0.1 wt% f-WS$_2$ and PAO6 + 1 wt% IL + 0.1 wt% f-SiO$_2$).
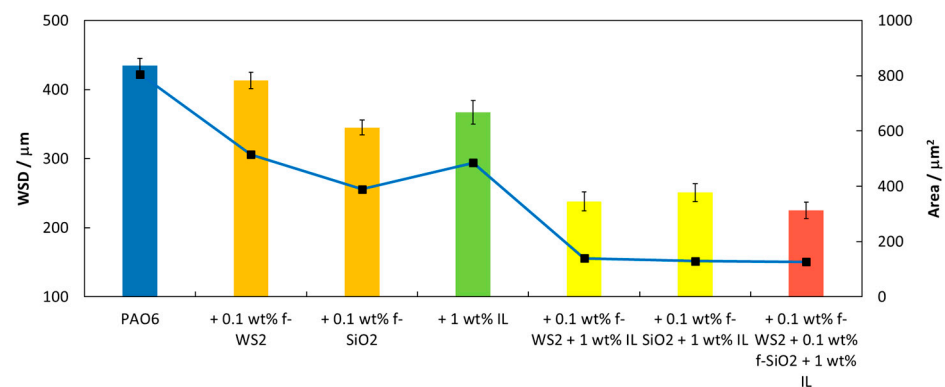


**Figure 7.** Wear scar diameters and areas of wear produced after tribological tests.
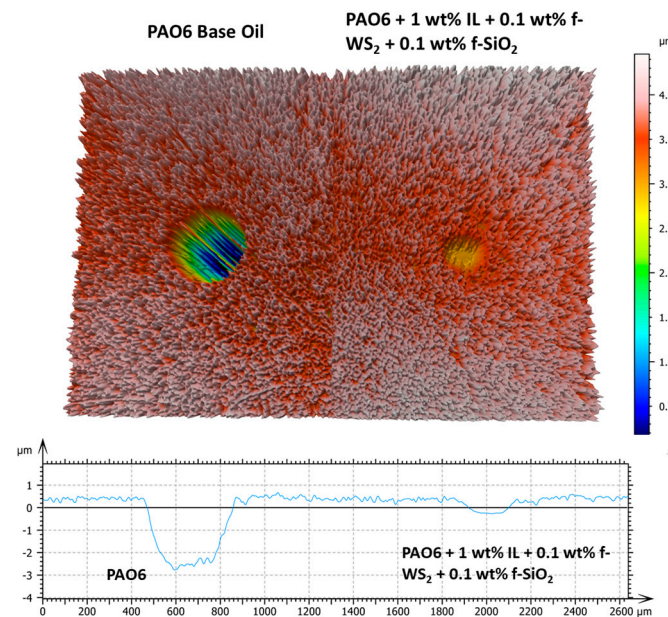
**Figure 8.** Three-dimensional worn profiles obtained with PAO6 and the optimal nanolubricant (double hybrid).

Roughness analyses (Ra and Rq) on worn surfaces tested with the different formulated lubricants were carried out, and they are presented in Table 3. It can be observed that the obtained roughness values for all the formulated nanolubricants are lower in comparison with the PAO6 base oil. Furthermore, the minimal roughness values were found for the double hybrid nanolubricant (PAO6 + 1 wt% IL + 0.1 wt% f-WS$_2$ + 0.1 wt% f-SiO$_2$) with a roughness drop of around 25%. This evidence indicates that, owing to the synergy between ILs and NPs in the contact, a more consistent surface could be observed after the pure sliding tests.

**Table 3.** Mean roughness values, Ra and Rq, with their uncertainties, σ, in worn pins studied with all lubricants.

| Lubricant | Ra/nm | σ | Rq/nm | σ |
|:---:|:---:|:---:|:---:|:---:|
| PAO6 | 11.2 | 1.4 | 15.3 | 2.4 |
| +0.1 wt% f-WS$_2$ | 11.1 | 1.2 | 14.7 | 2.3 |
| +0.1 wt% f-SiO$_2$ | 10.1 | 1.1 | 14.0 | 1.9 |
| +1 wt% IL | 11.2 | 1.3 | 15.2 | 2.5 |
| +0.1 wt% f-SiO$_2$ + 1 wt% IL | 9.3 | 1.1 | 13.2 | 1.8 |
| +0.1 wt% f-WS$_2$ + 1 wt% IL | 9.8 | 1.4 | 13.9 | 1.7 |
| +0.1 wt% f-WS$_2$ + 0.1 wt% f-SiO$_2$ + 1 wt% IL | 8.5 | 1.2 | 12.1 | 1.4 |

With the objective of understanding the role that NPs and IL play in the obtained friction and wear improvement, surface analysis was performed through Raman mapping of the worn surfaces achieved after the tribological friction tests. First, the Raman spectra of all the elements of PAO6-based nanolubricants (PAO base oil [42], the different NPs (Figure 4) and IL [22]) were collected to see the lubricant components in the mapping and therefore their distribution. So, mapping of the worn pins tested with the nanolubricant with the best antifriction and antiwear performance (PAO6 + 0.1 wt% f-WS$_2$ + 0.1 wt% f-SiO$_2$ + 1 wt% IL) was performed with a WITec alpha300R+ confocal Raman microscope (532 nm). Hence, Figure 9 reveals the Raman mapping of the worn pin tested with the PAO6 + 0.1 wt% f-WS$_2$ + 0.1 wt% f-SiO$_2$ + 1 wt% IL double hybrid nanolubricant. As can be seen in the Raman scheme, important areas in blue that are placed along the sliding furrows

coincide with the IL Raman spectrum. Furthermore, cyan and green areas that coincide with the f-WS$_2$ and f-SiO$_2$ Raman spectra, respectively, also appear in the Raman mapping. Regarding the f-WS$_2$ areas, it seems that some of them also appear in the sliding furrows direction. These facts suggest that tribofilm formation could occur due to the presence of IL, that small tribofilm formation and mending tribological mechanisms could happen on the worn surface due to f-WS$_2$ nanoparticles and finally that the presence of f-SiO$_2$ nanoparticles could lead to the occurrence of mending. These results are also supported by the previously shown roughness evaluation, where the roughness of the worn surface lubricated with the double hybrid nanolubricant was quite small in comparison with that obtained with the base oil without additives. In particular, the Ra inside the wear track lubricated with PAO8 has a value of 11.2 nm, whereas the one lubricated with the double hybrid nanolubricant has a Ra value of 8.5 nm, which indicates a roughness reduction of around 25%. These facts confirm that both NPs can cover the defects of the surface pins and act through a mending mechanism.
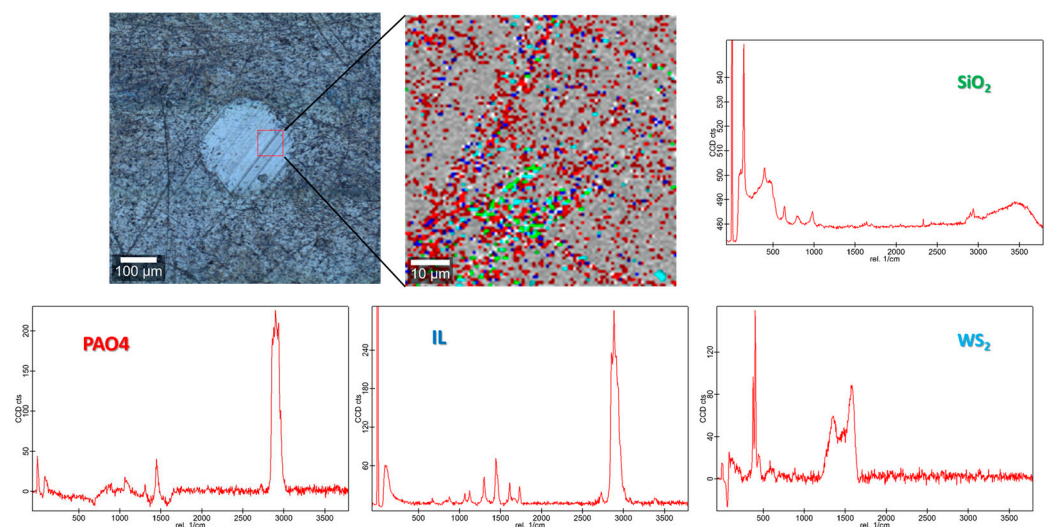


**Figure 9.** Raman mapping of worn surface tested with the optimal nanolubricant (+0.1 wt% f-WS$_2$ + 0.1 wt% f-SiO$_2$ + 1 wt% IL).

*3.2. Results of Rolling–Sliding Tests*

Rolling–sliding friction analyses for the PAO6 base oil and hybrid and double hybrid nanolubricants were also carried out at 120 °C. The sliding tests had an SRR of 5%, allowing for the completion of the Stribeck curves (Figures 10 and 11). The Stribeck curves were displayed by charting the friction coefficient versus the specific film thickness, $\Lambda$, which is calculated as follows:

$$\Lambda = \frac{h_t}{Rq} \tag{3}$$

where $h_t$ is the theoretical central film thickness and $Rq$ is the composite mean roughness of the two tribological surfaces (disc and ball) given by

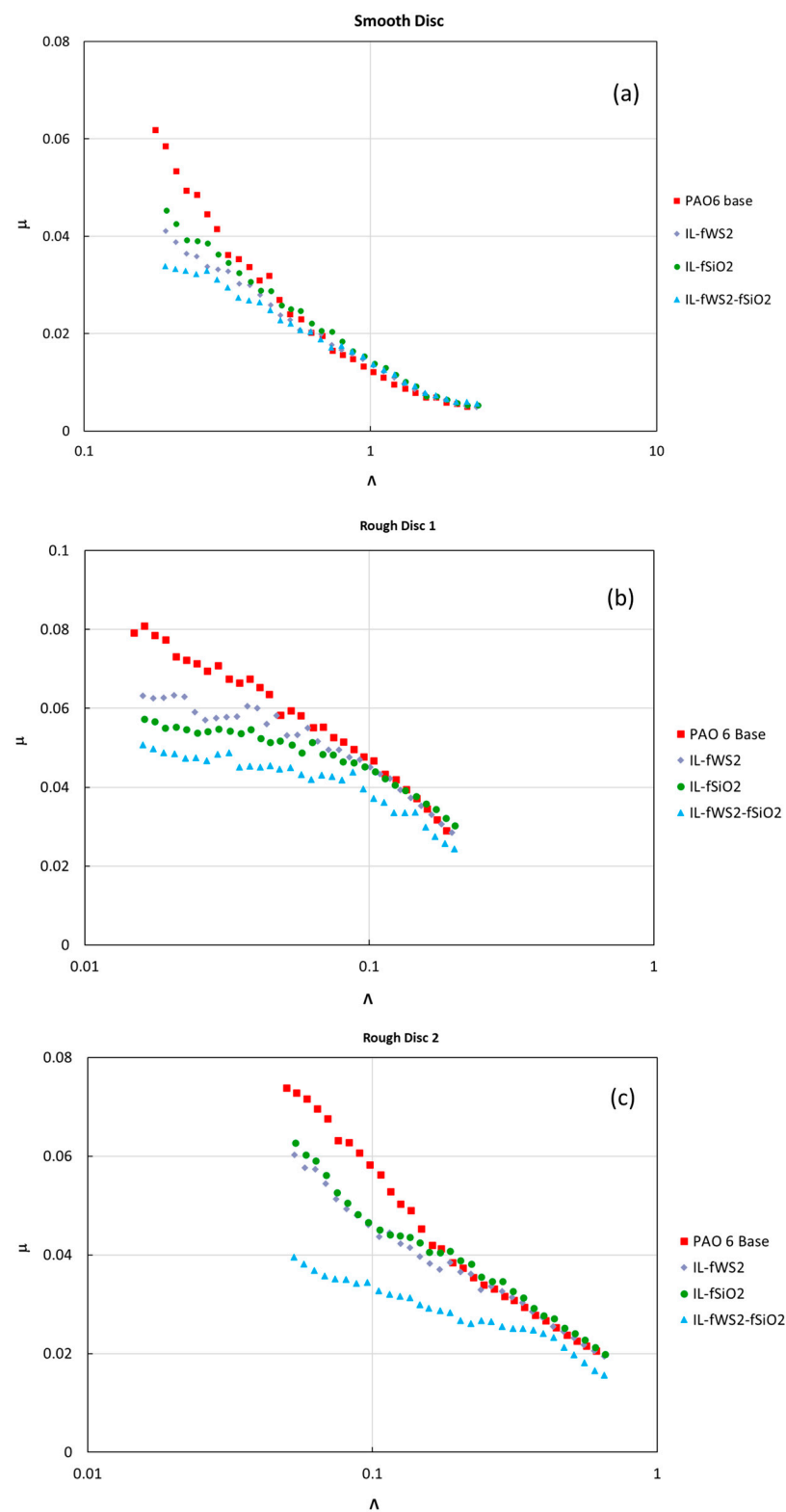$$Rq = \sqrt{(Rq_{disc})^2 + (Rq_{ball})^2}. \tag{4}$$

**Figure 10.** Stribeck curves of PAO6 and hybrid and double hybrid nanolubricants tested at 120 °C for the discs with different surface roughnesses: (**a**) smooth disc, (**b**) rough disc 1 and (**c**) rough disc 2.
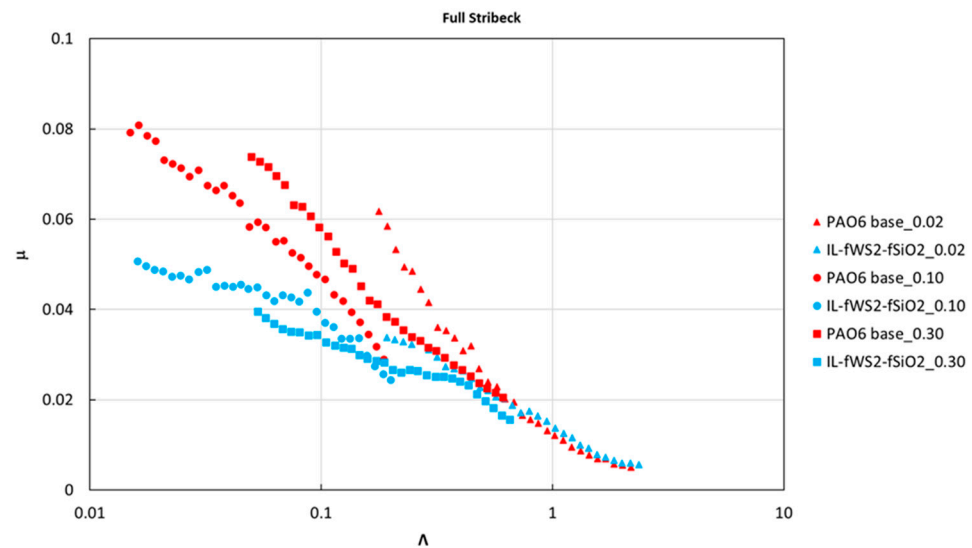
**Figure 11.** Full Stribeck curves of PAO6 (red) and double hybrid nanolubricant (blue) tested with the three discs at 120 °C and 5% SRR.

Regarding $h_t$ at 120 °C, it was estimated through the Hamrock and Downson's equation [43]. It should be noted that, for the approximation of $h_t$, the pressure−viscosity coefficient of PAO6 was utilized [44]. Furthermore, the viscosities of the nanolubricants and base oil were measured up to 100 °C by means of a Stabinger SVM3000 viscometer from Anton Paar (Table S1). Additionally, to correlate the measured viscosities, the Vogel−Fulcher−Tammann equation [44] was used to reach the dynamic viscosity of the nanolubricants and the PAO6 base oil at 120 °C, since the viscosimeter was not allowed to measure viscosities at temperatures higher than 100 °C.

All the achieved Stribeck curves are drawn in Figures 10 and 11 for the hybrid (PAO6 + 0.1 wt% f-WS$_2$ 1 wt% IL and PAO6 + 0.1 wt% f-SiO$_2$ + 1 wt% IL) and double hybrid (PAO6 + 0.1 wt% f-WS$_2$ + 0.1 wt% f-SiO$_2$ + 1 wt% IL) nanolubricants and PAO6 with the three discs with different roughnesses (Table 1). Figure 9 shows individually the friction behavior of the tested lubricants for each tried disc with different roughness surfaces. It can be obviously observed that the reached coefficients of friction were considerably reduced for the hybrid and double hybrid nanolubricants in relation to the PAO6 base oil. Particularly, the best antifriction behavior was achieved for the double hybrid nanolubricant for all the discs tested (Figure 10). The results in Figure 10 for each different disc are very important, since it can be seen that, for high specific film thicknesses (high speeds), the friction coefficient was reasonably comparable for all the nanolubricants and the PAO6 base oil. On the other hand, at quite low speeds (boundary lubrication), the effect of the NPs and IL addition was fundamental, helping to considerably decrease the friction, and the hydrodynamic effect was irrelevant.

Figure 11 shows the full Stribeck curve (three discs) for the PAO6 base oil and the optimal antifriction nanolubricant (PAO6 + 0.1 wt% f-WS$_2$ + 0.1 wt% f-SiO$_2$ + 1 wt% IL). As was assumed, in the rolling friction tests, the friction coefficient increased when the roughness of the discs rose, (Figure 11). It is well known that a full Stribeck curve is separated into different lubrication regimes: boundary, mixed, elastohydrodynamic and hydrodynamic, and full film lubrication. Based on different standards in the bibliography, boundary lubrication is determined when $\Lambda < 1$, mixed lubrication is determined when $1 < \Lambda < 3$, elastohydrodynamic lubrication (EHL) is determined when $\Lambda > 3$, and full film lubrication is determiend when $\Lambda > 5$. Based on the results found in Figure 11, the reached $\Lambda$ values occur between a minimum of around 0.02 (for the roughest disc) and a maximum of about 1.9 (the disc with minimal roughness). Accordingly, boundary film lubrication happened for all the discs studied, whereas mixed and full film lubrication specifically happened for the smoothest disc and at elevated speeds.

It should be noted that the wear generated in the disc and balls during these rolling–sliding tests could hardly be measured because it is practically non-existent due to small sliding.

## 4. Discussion

In this section, a discussion about the tribological mechanisms obtained in the pure sliding tribological tests is presented. The steel surfaces used as a tribopair (100Cr6 steel) in the pure sliding tests in this research were more chemically reactive than other metallic alloys; therefore, the decomposition of the IL, owing to the reaction with iron [45], could occur. The phosphonium IL used as a hybrid additive of lubricants had phosphorous as both an anion and cation; hence, it was not easy to conclude if the tribofilm formed was from the decomposition of the cation, the anion or both [46]. Furthermore, owing to the positive charge made by tribo-stress during tribological tests, anions usually tend to be adsorbed on the steel surface; therefore, this fact could control the lubricity of the IL [47]. In this vein, in a similar study carried out by Upendra and Vasu [24], who analyzed the tribological behavior of a phosphonium IL and three NPs as lubricant additives, they proved that the formation of a tribofilm rich in phosphate surfaces is responsible for improved triboperformances.

Regarding the other hybrid additive, f-$WS_2$, sulfur shows a significant function in the interaction between NPs and lubricant elements, since the heat produced by friction and high contact pressure could lead to a tribochemical reaction between NPs and their environments (lubricant, contacts. . .) [48]. Therefore, a tribofilm could be created on the friction worn surface. Here, tribofilm adsorption could be produced by f-$WS_2$ NPs, the lubricant and their chemically bonded elements. A similar effect was reported by Gullac and Akalin [49], who studied the tribological properties of IF-$WS_2$ nanoparticles as engine oil additives, finding that a thin tribofilm gradually forms on the piston ring surfaces, verified using Raman spectroscopy. The formation of a tribofilm is the most typical mechanism used to describe the antiwear and friction reduction performance of nanolubricants. Figure 12 shows a representation of the tribofilm formation in the tribological system used in this research, allowing for a better understanding of this tribological mechanism. Concerning the f-$SiO_2$ NPs, the tribological mechanism of mending obtained in this research was previously observed for these NPs in different research [21,50]. Thus, Sabarinath et al. [21], in similar research, evaluated the tribological synergies between two imidazolium ILs and $SiO_2$ NPs as hybrid additives, finding important enhancements due to the smaller size of $SiO_2$ nanoparticles, which can reduce friction and wear by mending and self-repairing mechanisms.
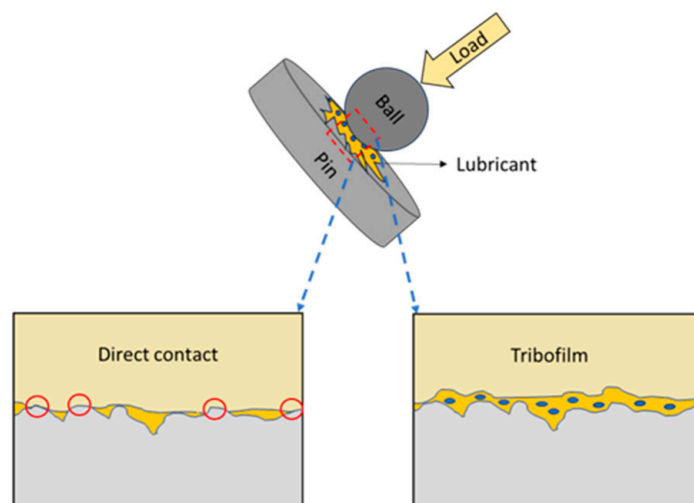


**Figure 12.** Representation of the tribofilm formation in the tribological pair.

### 5. Conclusions

Low-viscosity nanolubricants based on PAO6, a phosphonium IL and functionalized $WS_2$ and $SiO_2$ NPs as additives were tribologically studied to find possible synergistic effects between NPs and IL as additives, reaching the following conclusions:

- Good stability of nanolubricants was observed for the nanolubricants that contain IL, which acted as a dispersant.
- Friction coefficients reached with hybrid and double hybrid nanolubricants were smaller than those obtained for the PAO6 oil for all tribological tests (pure sliding and rolling-sliding).
- The biggest friction reductions in pure sliding tests were achieved for PAO6 + 1 wt% IL + 0.1 wt% f-$WS_2$ + 0.1 wt% f-$SiO_2$ with a maximum friction reduction of 25%, therefore observing antifriction synergies.
- All the tested nanolubricants exhibited enhanced antiwear performance in comparison to PAO6. The PAO6 + 1 wt% IL + 0.1 wt% f-$WS_2$ + 0.1 wt% f-$SiO_2$ nanolubricant achieved the best antiwear performance, with width and area reductions of 48% and 84%, respectively.
- The roughness of worn surfaces lubricated with the double hybrid nanolubricant was quite low in comparison with that tested with the base oil without additives, with a roughness reduction of around 25%.
- From the Raman mappings and roughness evaluations of worn pin surfaces studied in pure sliding conditions, it is proposed that the tribological mechanism of lubrication for double hybrid nanolubricants could be supported by the adsorbed tribofilm (IL and f-$WS_2$) as well as the mending effects (f-$WS_2$ and f-$SiO_2$).
- Concerning the rolling–sliding tests, NPs and IL played a crucial role in the extreme boundary lubrication regime, considerably reducing the friction coefficient.
- The developed low-viscosity nanolubricants with excellent antifriction and antiwear properties were found as potential transmission fluids for the EV industry.

**Supplementary Materials:** The following supporting information can be downloaded at https://www.mdpi.com/article/10.3390/lubricants12020058/s1: Table S1: Dynamic viscosities of PAO6-based nanolubricants and PAO6 base oil.

**Author Contributions:** Conceptualization, J.M.L.d.R.; methodology, J.M.L.d.R. and C.M.C.G.F.; software, D.E.P.G. and C.M.C.G.F.; validation, C.M.C.G.F., D.E.P.G. and J.H.O.S.; formal analysis, J.M.L.d.R.; investigation, J.M.L.d.R.; resources, C.M.C.G.F. and J.H.O.S.; data curation, J.M.L.d.R.; writing—original draft preparation, J.M.L.d.R.; writing—review and editing, J.M.L.d.R., D.E.P.G., C.M.C.G.F. and J.H.O.S.; visualization, D.E.P.G.; supervision, J.H.O.S.; project administration, J.H.O.S. and C.M.C.G.F.; funding acquisition, J.H.O.S. and C.M.C.G.F. All authors have read and agreed to the published version of the manuscript.

**Data Availability Statement:** Data are contained within the article.

**Conflicts of Interest:** The authors declare no conflict of interest.

### References

1. Holmberg, K.; Erdemir, A. The impact of tribology on energy use and $CO_2$ emission globally and in combustion engine and electric cars. *Tribol. Int.* **2019**, *135*, 389–396. [CrossRef]
2. Gupta, A. Characterization of Engine and Transmission Lubricants for Electric, Hybrid, and Plug-In Hybrid Vehicles. Ph.D. Thesis, Ohio State University, Columbus, OH, USA, 2012.

3.  Aguilar-Rosas, O.A.; Alvis-Sánchez, J.A.; Tormos, B.; Marín-Santibáñez, B.M.; Pérez-González, J.; Farfan-Cabrera, L.I. Enhancement of low-viscosity synthetic oil using graphene nanoparticles as additives for enduring electrified tribological environments. *Tribol. Int.* **2023**, *188*, 108848. [CrossRef]

4.  Ahmed Abdalglil Mustafa, W.; Dassenoy, F.; Sarno, M.; Senatore, A. A review on potentials and challenges of nanolubricants as promising lubricants for electric vehicles. *Lubr. Sci.* **2022**, *34*, 1–29. [CrossRef]

5.  Mariño, F.; Liñeira del Río, J.M.; López, E.R.; Fernández, J. Chemically modified nanomaterials as lubricant additive: Time stability, friction, and wear. *J. Mol. Liq.* **2023**, *382*, 121913. [CrossRef]

6.  Gulzar, M.; Masjuki, H.H.; Kalam, M.A.; Varman, M.; Zulkifli, N.W.M.; Mufti, R.A.; Zahid, R. Tribological performance of nanoparticles as lubricating oil additives. *J. Nanoparticle Res.* **2016**, *18*, 223. [CrossRef]

7.  Singh, A.; Chauhan, P.; Mamatha, T.G. A review on tribological performance of lubricants with nanoparticles additives. *Mater. Today Proc.* **2020**, *25*, 586–591. [CrossRef]

8.  Liñeira del Río, J.M.; Alba, A.; Guimarey, M.J.G.; Prado, J.I.; Amigo, A.; Fernández, J. Surface tension, wettability and tribological properties of a low viscosity oil using $CaCO_3$ and $CeF_3$ nanoparticles as additives. *J. Mol. Liq.* **2023**, *391*, 123188. [CrossRef]

9.  Mu, Z.; Zhou, F.; Zhang, S.; Liang, Y.; Liu, W. Effect of the functional groups in ionic liquid molecules on the friction and wear behavior of aluminum alloy in lubricated aluminum-on-steel contact. *Tribol. Int.* **2005**, *38*, 725–731. [CrossRef]

10. Qu, J.; Truhan, J.J.; Dai, S.; Luo, H.; Blau, P.J. Ionic liquids with ammonium cations as lubricants or additives. *Tribol. Lett.* **2006**, *22*, 207–214. [CrossRef]

11. Kheireddin, B.A.; Lu, W.; Chen, I.C.; Akbulut, M. Inorganic nanoparticle-based ionic liquid lubricants. *Wear* **2013**, *303*, 185–190. [CrossRef]

12. Avilés, M.-D.; Saurín, N.; Sanes, J.; Carrión, F.-J.; Bermúdez, M.-D. Ionanocarbon Lubricants. The Combination of Ionic Liquids and Carbon Nanophases in Tribology. *Lubricants* **2017**, *5*, 14. [CrossRef]

13. Zhou, Y.; Qu, J. Ionic Liquids as Lubricant Additives: A Review. *ACS Appl. Mater. Interfaces* **2017**, *9*, 3209–3222. [CrossRef]

14. Otero, I.; López, E.R.; Reichelt, M.; Villanueva, M.; Salgado, J.; Fernández, J. Ionic Liquids Based on Phosphonium Cations As Neat Lubricants or Lubricant Additives for a Steel/Steel Contact. *ACS Appl. Mater. Interfaces* **2014**, *6*, 13115–13128. [CrossRef]

15. Zhou, Y.; Dyck, J.; Graham, T.W.; Luo, H.; Leonard, D.N.; Qu, J. Ionic Liquids Composed of Phosphonium Cations and Organophosphate, Carboxylate, and Sulfonate Anions as Lubricant Antiwear Additives. *Langmuir* **2014**, *30*, 13301–13311. [CrossRef]

16. Liñeira del Río, J.M.; López, E.R.; García, F.; Fernández, J. Tribological synergies among chemical-modified graphene oxide nanomaterials and a phosphonium ionic liquid as additives of a biolubricant. *J. Mol. Liq.* **2021**, *336*, 116885. [CrossRef]

17. Khare, V.; Pham, M.-Q.; Kumari, N.; Yoon, H.-S.; Kim, C.-S.; Park, J.-I.L.; Ahn, S.-H. Graphene–Ionic Liquid Based Hybrid Nanomaterials as Novel Lubricant for Low Friction and Wear. *ACS Appl. Mater. Interfaces* **2013**, *5*, 4063–4075. [CrossRef] [PubMed]

18. Zhang, L.; Pu, J.; Wang, L.; Xue, Q. Synergistic Effect of Hybrid Carbon Nanotube–Graphene Oxide as Nanoadditive Enhancing the Frictional Properties of Ionic Liquids in High Vacuum. *ACS Appl. Mater. Interfaces* **2015**, *7*, 8592–8600. [CrossRef] [PubMed]

19. Liñeira del Río, J.M.; López, E.R.; Fernández, J. Synergy between boron nitride or graphene nanoplatelets and tri(butyl) ethylphosphonium diethylphosphate ionic liquid as lubricant additives of triisotridecyltrimellitate oil. *J. Mol. Liq.* **2020**, *301*, 112442. [CrossRef]

20. Maurya, U.; Vasu, V.; Kashinath, D. Ionic Liquid-Nanoparticle-Based Hybrid-Nanolubricant Additives for Potential Enhancement of Tribological Properties of Lubricants and Their Comparative Study with ZDDP. *Tribol. Lett.* **2022**, *70*, 11. [CrossRef]

21. Sabarinath, S.; Rajendrakumar, P.; Prabhakaran Nair, K. Evaluation of tribological properties of sesame oil as biolubricant with $SiO_2$ nanoparticles and imidazolium-based ionic liquid as hybrid additives. *Proc. Inst. Mech. Eng. Part J J. Eng. Tribol.* **2019**, *233*, 1306–1317. [CrossRef]

22. Nasser, K.I.; Liñeira del Río, J.M.; López, E.R.; Fernández, J. Synergistic effects of hexagonal boron nitride nanoparticles and phosphonium ionic liquids as hybrid lubricant additives. *J. Mol. Liq.* **2020**, *311*, 113343. [CrossRef]

23. Nasser, K.I.; Liñeira del Río, J.M.; Mariño, F.; López, E.R.; Fernández, J. Double hybrid lubricant additives consisting of a phosphonium ionic liquid and graphene nanoplatelets/hexagonal boron nitride nanoparticles. *Tribol. Int.* **2021**, *163*, 107189. [CrossRef]

24. Upendra, M.; Vasu, V. Synergistic Effect Between Phosphonium-Based Ionic Liquid and Three Oxide Nanoparticles as Hybrid Lubricant Additives. *J. Tribol.* **2020**, *142*, 052101. [CrossRef]

25. Nasser, K.I.; Liñeira del Río, J.M.; López, E.R.; Fernández, J. Hybrid combinations of graphene nanoplatelets and phosphonium ionic liquids as lubricant additives for a polyalphaolefin. *J. Mol. Liq.* **2021**, *336*, 116266. [CrossRef]

26. Kumar, G.; Garg, H.C. Tribological evaluation of rice bran oil based ionanolubricants containing ionic liquids and nanoparticles. *Tribol.-Mater. Surf. Interfaces* **2023**, *17*, 217–223. [CrossRef]

27. Hu, N.; Zhang, X.; Wang, X.; Wu, N.; Wang, S. Study on Tribological Properties and Mechanisms of Different Morphology $WS_2$ as Lubricant Additives. *Materials* **2020**, *13*, 1522. [CrossRef] [PubMed]

28. Lu, Z.; Cao, Z.; Hu, E.; Hu, K.; Hu, X. Preparation and tribological properties of $WS_2$ and $WS_2/TiO_2$ nanoparticles. *Tribol. Int.* **2019**, *130*, 308–316. [CrossRef]

29. Hamisa, A.H.; Azmi, W.H.; Ismail, M.F.; Rahim, R.A.; Ali, H.M. Tribology Performance of Polyol-Ester Based $TiO_2$, $SiO_2$, and Their Hybrid Nanolubricants. *Lubricants* **2023**, *11*, 18. [CrossRef]

30. Cortes, V.; Sanchez, K.; Gonzalez, R.; Alcoutlabi, M.; Ortega, J.A. The Performance of SiO$_2$ and TiO$_2$ Nanoparticles as Lubricant Additives in Sunflower Oil. *Lubricants* **2020**, *8*, 10. [CrossRef]

31. Mariño, F.; Liñeira del Río, J.M.; Gonçalves, D.E.P.; Seabra, J.H.O.; López, E.R.; Fernández, J. Effect of the addition of coated SiO$_2$ nanoparticles on the tribological behavior of a low-viscosity polyalphaolefin base oil. *Wear* **2023**, *530–531*, 205025. [CrossRef]

32. Wu, J.; Yue, G.; Xiao, Y.; Huang, M.; Lin, J.; Fan, L.; Lan, Z.; Lin, J.-Y. Glucose Aided Preparation of Tungsten Sulfide/Multi-Wall Carbon Nanotube Hybrid and Use as Counter Electrode in Dye-Sensitized Solar Cells. *ACS Appl. Mater. Interfaces* **2012**, *4*, 6530–6536. [CrossRef]

33. Latha, M.; Vatsala Rani, J. WS$_2$/Graphene Composite as Cathode for Rechargeable Aluminum-Dual Ion Battery. *J. Electrochem. Soc.* **2020**, *167*, 070501. [CrossRef]

34. Hu, Q.; Suzuki, H.; Gao, H.; Araki, H.; Yang, W.; Noda, T. High-frequency FTIR absorption of SiO$_2$/Si nanowires. *Chem. Phys. Lett.* **2003**, *378*, 299–304. [CrossRef]

35. Budiarti, H.; Puspitasari, R.; Hatta, A.; Koentjoro, S.; Risanti, D. Synthesis and Characterization of TiO$_2$@SiO$_2$ and SiO$_2$@TiO$_2$ Core-Shell Structure Using Lapindo Mud Extract via Sol-Gel Method. *Procedia Eng.* **2017**, *170*, 65–71. [CrossRef]

36. Berkdemir, A.; Gutiérrez, H.R.; Botello-Méndez, A.R.; Perea-López, N.; Elías, A.L.; Chia, C.-I.; Wang, B.; Crespi, V.H.; López-Urías, F.; Charlier, J.-C.; et al. Identification of individual and few layers of WS$_2$ using Raman Spectroscopy. *Sci. Rep.* **2013**, *3*, 1755. [CrossRef]

37. Lee, E.L.; Wachs, I.E. In Situ Raman Spectroscopy of SiO$_2$-Supported Transition Metal Oxide Catalysts: An Isotopic $^{18}$O$-^{16}$O Exchange Study. *J. Phys. Chem. C* **2008**, *112*, 6487–6498. [CrossRef]

38. Liñeira del Río, J.M.; López, E.R.; González Gómez, M.; Yáñez Vilar, S.; Piñeiro, Y.; Rivas, J.; Gonçalves, D.E.P.; Seabra, J.H.O.; Fernández, J. Tribological Behavior of Nanolubricants Based on Coated Magnetic Nanoparticles and Trimethylolpropane Trioleate Base Oil. *Nanomaterials* **2020**, *10*, 683. [CrossRef]

39. Hamrock, B.J.; Schmid, S.R.; Jacobson, B.O. *Fundamentals of Fluid Film Lubrication*, 2nd ed.; CRC Press: Boca Raton, FL, USA, 2004. [CrossRef]

40. Petzold, C.; Koch, M.; Bennewitz, R. Friction force microscopy of tribochemistry and interfacial ageing for the SiO$_x$/Si/Au system. *Beilstein J. Nanotechnol.* **2018**, *9*, 1647–1658. [CrossRef]

41. Vorholzer, M.; Vilhena, J.G.; Perez, R.; Gnecco, E.; Dietzel, D.; Schirmeisen, A. Temperature Activates Contact Aging in Silica Nanocontacts. *Phys. Rev. X* **2019**, *9*, 041045. [CrossRef]

42. Liñeira del Río, J.M.; Mariño, F.; López, E.R.; Gonçalves, D.E.P.; Seabra, J.H.O.; Fernández, J. Tribological enhancement of potential electric vehicle lubricants using coated TiO$_2$ nanoparticles as additives. *J. Mol. Liq.* **2023**, *371*, 121097. [CrossRef]

43. Hamrock, B.; Dowson, D. Minimum Film Thickness in Elliptical Contacts for Different Regimes of Fluid-Film Lubrication. 1978. Available online: https://ntrs.nasa.gov/citations/19780025504 (accessed on 21 January 2024).

44. Gonçalves, D.E.P.; Liñeira del Rio, J.M.; Comuñas, M.J.P.; Fernández, J.; Seabra, J.H.O. High Pressure Characterization of the Viscous and Volumetric Behavior of Three Transmission Oils. *Ind. Eng. Chem. Res.* **2019**, *58*, 1732–1742. [CrossRef]

45. Bermúdez, M.-D.; Jiménez, A.-E.; Sanes, J.; Carrión, F.-J. Ionic Liquids as Advanced Lubricant Fluids. *Molecules* **2009**, *14*, 2888–2908. [CrossRef] [PubMed]

46. Li, H.; Somers, A.E.; Howlett, P.C.; Rutland, M.W.; Forsyth, M.; Atkin, R. Addition of low concentrations of an ionic liquid to a base oil reduces friction over multiple length scales: A combined nano- and macrotribology investigation. *Phys. Chem. Chem.* **2016**, *18*, 6541–6547. [CrossRef]

47. Li, Y.; Zhang, S.; Ding, Q.; Li, H.; Qin, B.; Hu, L. Understanding the synergistic lubrication effect of 2-mercaptobenzothiazolate based ionic liquids and Mo nanoparticles as hybrid additives. *Tribol. Int.* **2018**, *125*, 39–45. [CrossRef]

48. Dai, W.; Kheireddin, B.; Gao, H.; Liang, H. Roles of nanoparticles in oil lubrication. *Tribol. Int.* **2016**, *102*, 88–98. [CrossRef]

49. Gullac, B.; Akalin, O. Frictional Characteristics of IF-WS$_2$ Nanoparticles in Simulated Engine Conditions. *Tribol. Trans.* **2010**, *53*, 939–947. [CrossRef]

50. Peng, D.X.; Kang, Y.; Hwang, R.M.; Shyr, S.S.; Chang, Y.P. Tribological properties of diamond and SiO$_2$ nanoparticles added in paraffin. *Tribol. Int.* **2009**, *42*, 911–917. [CrossRef]